Steel and Composite Structures, *Vol. 32, No. 5 (2019) 687-699*
DOI: https://doi.org/10.12989/scs.2019.32.5.687

Semi-analytical solutions of free and force vibration behaviors of GRC-FG cylindrical shells

Zuxiang Lei* and Lihong Tong

Institute of Geotechnical Engineering, School of Civil Engineering and Architecture, East China Jiaotong University, Nanchang, 330013, Jiangxi, P.R. China

(*Received April 29, 2019, Revised July 30, 2019, Accepted August 3, 2019*)

Abstract. In this paper, free and force vibration behaviors of graphene-reinforced composite functionally graded (GRC-FG) cylindrical shells in thermal environments are investigated based on Reddy's third-order shear deformation theory (HSDT). The GRC-FG cylindrical shells are composed of piece-wise pattern graphene-reinforced layers which have different volume fraction. Based on the extended Halpin-Tsai micromechanical model, the effective material properties of the resulting nanocomposites are evaluated. Using the Hamilton's principle and the assumed mode method, the motion equation of the GRC-FG cylindrical shells is formulated. Using the time- and frequency-domain methods, free and force vibration properties of the GRC-FG cylindrical shell are analyzed. Numerical cases are provided to study the effects of distribution of graphene, shell radius-to-thickness ratio and temperature changes on the free and force vibration responses of GRC-FG cylindrical shells.

Keywords: vibration; graphene; HSDT; extended Halpin-Tsai model; analytical modeling

1. Introduction

Nano-composites, as a new type advance material, have become as one of the hottest research topics in recent years. Nano-composites have the potential to be used in civil industry, but also for military, such as in aerospace industry. Such as for carbon nanotube reinforced composites, many investigations have been carried out. Liew *et al*. (2015) presented comprehensive review of mechanical analysis, such static, dynamic, linear and nonlinear and so on, of functionally graded carbon nanotube reinforced composites. Bahrami *et al*. (2018) investigated nonlinear forced vibration of FG-CNTs-reinforced curved microbeam based on strain gradient theory considering out-of-plane motion. Arani *et al*. (2018) presented buckling and free vibration analysis of sandwich micro plate (SMP) integrated with piezoelectric layers embedded in orthotropic Pasternak. Lei and Zhang (2018) examined the effect of matrix cracks on the buckling of a hybrid laminated plate which is composed of carbon nanotube reinforced functionally graded (CNTR-FG) layers and conventional fiber reinforced composite (FRC) layers. Tahouneh (2018) studied the influence of carbon nanotubes (CNTs) waviness and aspect ratio on the vibrational behavior of functionally graded nanocomposite sandwich annular sector plates resting on two-parameter elastic foundations. Asadi and Beheshti (2018) investigated the nonlinear dynamic responses of FG-CNTRC beams exposed to axial supersonic airflow based on third-order piston theory. Vertuccio *et al*. (2017) designed and characterized new electrically conductive adhesives based on Multi Wall Carbon Nanotubes (MWCNTs) and functionalized liquid rubber. The results showed that the inclusion of MWCNTs in the toughened adhesive can be advantageously employed for further enhancing adhesive properties simultaneously imparting electrical conductivity, which results of 11 orders of magnitude higher than the unfilled formulation. Mehri *et al*. (2016a) reported the bifurcation and vibration responses of a composite truncated conical shell with embedded SWCNTs. Gul and Aydogdu (2018) investigated free vibration and buckling of double-walled carbon nanotubes embedded in an elastic medium with simply supported boundary conditions using Doublet Mechanics. Jensen *et al*. (2018) investigated the effects of carbon nanotube continuity and interfacial bonding on composite strength and stiffness. Fantuzzi *et al*. (2017) conducted free vibration analysis of arbitrarily shaped Functionally Graded Carbon Nanotube-reinforced plates. Ansari *et al*. (2017) presented the buckling and vibration analysis of thermally pre-stressed functionally graded carbon-nanotube-reinforced composite annular sector plates resting on the elastic foundation via the variational differential quadrature method. Shen *et al*. (2017) investigated the small- and large-amplitude vibrations of thermally postbuckled carbon nanotube-reinforced composite beams resting on elastic foundations. Liew *et al*. (2014) examined the postbuckling behaviors of carbon nanotube-reinforced functionally graded cylindrical panels under axial compression using a meshless approach. Song *et al*. (2016a, b) analytically investigated the dynamic responses of CNT composite plates subjected to impact loading and the active vibration control of carbon nanotube reinforced functionally graded plates using piezoelectric actuator and sensor pairs bonded on the top and bottom

*Corresponding author, Ph.D., Professor,
E-mail: leizux@njust.edu.cn

ISSN: 1229-9367 (Print), 1598-6233 (Online)

surfaces of the host plate based on Reddy's high-order shear deformation theory. Mehri *et al*. (2016b), Asadi (2017), Asadi *et al*. (2017), Asadi and Wang (2017a, b), Keleshteri *et al*. (2017a, b), Mehri *et al*. (2017), Mohammadzadeh-Keleshteri *et al*. (2017), Keleshteri *et al*. (2018, 2019) presented a comprehensive study about the linear, non-linear, static, dynamic investigations of FG-CNTRC beam, plate and shell. Tornabene *et al*. (2018) presented the application of the first-order shear deformation theory (FSDT) to thermo-elastic static problems of functionally graded carbon nanotubes reinforced composite (FG-CNTRC) cylindrical pressure vessels. Yang *et al*. (2018) investigated the free vibration of geometrically imperfect functionally graded car-bon nanotube-reinforced composite (FG-CNTRC) beams. Kumar and Srinivas (2018) presented the transient vibration behavior of functionally graded carbon nanotube (FG-CNT) reinforced nanocomposite plate resting on Pasternak foundation under pulse excitation.

Recently, graphene reinforced composites (GRCs), as advanced composite materials, attract much attention from researchers. Rafiee *et al*. (2009) presented an experimental study on buckling of graphene/epoxy nanocomposite beam structures. Their results showed that significant increase (up to 52%) in critical buckling load was observed with addition of only 0.1% weight fraction of graphene platelets into the epoxy matrix. An efficient strategy to achieve a high alignment of graphene nanosheets (GNSs) in GNS/Cu composites through a vacuum filtration method was reported Chu *et al*. (2018). Feng *et al*. (2017) studied the nonlinear bending behavior of a novel class of multi-layer polymer nanocomposite beams reinforced with graphene platelets (GPLs) that are non-uniformly distributed along the thickness direction. Wan *et al*. (2018) synthesized Nano-silicon/graphene composites directly from silicon and graphite mixture as the raw materials with one-step process under atmospheric pressure by thermal plasma approach. Using molecular dynamics (MD) methods, Zhan *et al*. (2017) studied the mechanical properties of the SiC/graphene composites under tensile. Lei *et al*. (2018) investigated buckling behavior of graphene-reinforced composite functionally graded laminated plates. The small and large amplitude vibration behaviors of graphene-reinforced composite laminated cylindrical panels supported was studied by Shen *et al*. (2018). Kiani (2018) proposed a nonlinear formulation to study the large amplitude free vibration of composite laminated plates reinforced by graphene sheets. Hosseini and Zhang (2018) examined the transient dynamic analysis and elastic wave propagation in a functionally graded graphene platelets (FGGPLs)-reinforced composite thick hollow cylinder.

Closed cylindrical shells are very common and important structures in mechanical and civil engineering. In the literature, there are many investigations about vibration behaviors of closed cylindrical shells. Zhang *et al*. (2001) presented the vibration analysis of cylindrical shells using wave propagation method. Zhang *et al*. (2018) proposed a modified Fourier cosine series method for beams and plates for free vibration analysis of moderately thick cylindrical shell with general boundary conditions. Harbaoui *et al*. (2018) presented a new spectral element based on the dynamic stiffness matrix of a prestressed cylindrical shell. Shakouri and Kouchakzadeh (2017) proposed a simple analytical method for determination of natural frequencies of generally laminated conical and cylindrical shells with arbitrary boundary conditions. Sofiyev *et al*. (2017) examined the non-linear free vibration behavior of functionally graded orthotropic cylindrical shell interacting with the two-parameter elastic foundation. Liew *et al*. (2012) presented a postbuckling analysis of functionally graded cylindrical shells under axial compression and thermal loads using the element-free kp-Ritz method.

Therefore, in this paper free and force vibration behaviors of graphene-reinforced composite functionally graded (GRC-FG) cylindrical shells in thermal environments are investigated based on Reddy's third-order shear deformation theory (HSDT). The GRC-FG cylindrical shells are composed of piece-wise pattern graphene-reinforced layers which have different volume fraction. Based on the extended Halpin-Tsai micromechanical model, the effective material properties of the resulting nanocomposites are evaluated. The motion equation of the GRC-FG cylindrical shells is formulated using the Hamilton's principle and the assumed mode method. Free and force vibration properties of the GRC-FG cylindrical shell are analyzed based the time- and frequency-domain methods. Numerical cases are provided to study the effects of distribution of graphene, shell radius-to-thickness ratio and temperature changes on the free and force vibration responses of GRC-FG cylindrical shells.

2. GRC-FG cylindrical shells

As shown in Fig. 1(a), GRC-FG cylindrical shells with geometry properties as radius R, thickness h and length L are considered in this paper. The GRC-FG cylindrical shells are composed of the Piece-wise distribution types of GRCs layers. Three types of GRC-FG cylindrical shells, UD, FG-O and FG-X, are shown in Fig. 1(b). The volume fractions of graphene of GRCs layers for UD, FG-O and FG-X GRC-FG cylindrical shells are given [(0.07)/ (0.07)/ (0.07)/ (0.07)/ (0.07)/ (0.07)/ (0.07)/ (0.07)/ (0.07)/ (0.07; [(0.03)/ (0.05)/ (0.07)/ (0.09)/ (0.11)/ (0.11)/ (0.09)/ (0.07)/ (0.05)/ (0.03)]; [(0.11)/ (0.09)/ (0.07)/ (0.05)/ (0.03)/ (0.03)/ (0.05)/ (0.07)/ (0.09)/ (0.11)]. For the present GRC-FG cylindrical shells, the effective material properties are evaluated according to the extended Halpin-Tsai mode Shen *et al*. (2018). The Young's modulus and shear modulus are given as

$$E_{11} = \eta_1 \frac{1 + (2\, a_G / h_G)\gamma_{11} V_G}{1 - \gamma_{11} V_G} E^m \tag{1}$$

$$E_{22} = \eta_2 \frac{1 + (2\, a_G / h_G)\gamma_{22} V_G}{1 - \gamma_{22} V_G} E^m \tag{2}$$

$$G_{12} = \eta_3 \frac{1}{1 - \gamma_{12} V_G} G^m \tag{3}$$

where a_G, b_G and h_G are geometric parameters of the

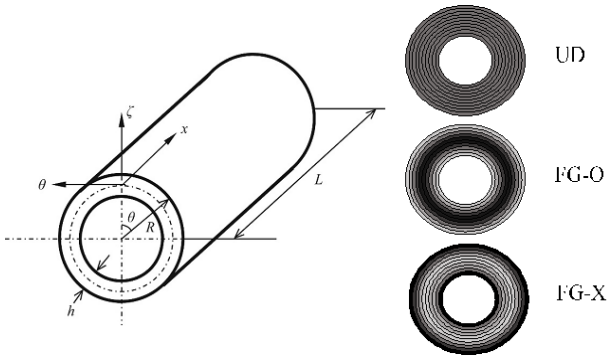

(a) (b)

Fig. 1 (a) Schematic diagram of GRC-FG cylindrical shell; (b) Configurations of GRC layers in the thickness direction

graphene sheet. In Eqs. (1)-(3), a new parameter η_j (j = 1, 2, 3), which are called the graphene efficiency parameters are introduced to consider the scale effect. The value of η_j (j = 1, 2, 3) can be determined by matching the material properties of GRCs predicted from the traditional Halpin-Tsai model to results from the MD simulations of Shen *et al*. (2018)

$$\gamma_{11} = \frac{E_{11}^G/E^m - 1}{E_{11}^G/E^m + 2\,a_G/h_G} \tag{4}$$

$$\gamma_{22} = \frac{E_{22}^G/E^m - 1}{E_{22}^G/E^m + 2\,b_G/h_G} \tag{5}$$

$$\gamma_{12} = \frac{G_{12}^G/G^m - 1}{G_{12}^G/G^m} \tag{6}$$

where E_{11}^G, E_{22}^G and G_{12}^G are the Young's moduli and shear modulus of the graphene sheet, and E^m and G^m are the corresponding Young's moduli and shear modulus of the. The volume fractions of graphene and matrix are defined as V_G and $V_m = 1 - V_G$, respectively. The Poisson's ratio is defined as

$$\upsilon_{12} = V_G\upsilon_{12+}^G V_m\upsilon^m \tag{7}$$

where υ_{12}^G and υ^m are the Poisson's ratios of the graphene and matrix, respectively.

The longitudinal and transverse thermal expansion coefficients of GRC-FG cylindrical shells can be shown as follow

$$\alpha_{11} = \frac{V_G E_{11}^G \alpha_{11}^G + V_m E^m \alpha^m}{V_G E_{11}^G + V_m E^m} \tag{8}$$

$$\alpha_{22} = (1+\upsilon_{12}^G)V_G\alpha_{11}^G + (1+\upsilon_m)V_m\alpha^m - \upsilon_{12}\alpha_{11} \tag{9}$$

α_{11}^G, α_{22}^G and α^m are the thermal expansion coefficients of graphene and matrix.

3. Formulation of motion

The displacement field of GRC-FG cylindrical shells are expressed based Reddy's third-order shear deformation theory by Reddy (1999)

$$u = u_0 + \zeta\phi_x - \frac{4}{3h^2}\zeta^3\left(\phi_x + \frac{\partial w_0}{\partial x}\right) \tag{10}$$

$$v = \left(1+\frac{\zeta}{R}\right)v_0 + \zeta\phi_y - \frac{4}{3h^2}\zeta^3\left(\phi_y + \frac{1}{R}\frac{\partial w_0}{\partial y}\right) \tag{11}$$

$$w = w_0 \tag{12}$$

where (u_0, v_o, w_0, ϕ_x, ϕ_y) are the displacement components of the neutral plane, and are the rotations of the transverse normal about q and x axes. z is the transverse coordinate.

The strain components and strain-displacement of GRC-FG cylindrical shells are given as Gong *et al*. (1994)

$$\boldsymbol{\varepsilon} = \boldsymbol{\varepsilon_0} + \zeta\boldsymbol{\kappa}_1 + \zeta^3\boldsymbol{\kappa}_3 \tag{13}$$

$$\boldsymbol{\gamma} = \boldsymbol{\gamma}_0 + \zeta^2\boldsymbol{\gamma}_2 \tag{14}$$

$$\boldsymbol{\varepsilon}_0 = \begin{Bmatrix} \dfrac{\partial u_0}{\partial x} \\ \dfrac{1}{R}\dfrac{\partial v_0}{\partial\theta} + \dfrac{w}{R} \\ \dfrac{\partial v_0}{\partial x} + \dfrac{1}{R}\dfrac{\partial u_0}{\partial\theta} \end{Bmatrix}, \quad \boldsymbol{\kappa}_1 = \begin{Bmatrix} \dfrac{\partial\phi_x}{\partial x} \\ \dfrac{1}{R}\dfrac{\partial\phi_y}{\partial\theta} \\ \dfrac{\partial\phi_y}{\partial x} + \dfrac{1}{R}\dfrac{\partial\phi_x}{\partial\theta} \end{Bmatrix} \tag{15}$$

$$\boldsymbol{\kappa}_3 = -c_1\begin{Bmatrix} \dfrac{\partial\phi_x}{\partial x} + \dfrac{\partial^2 w_0}{\partial x^2} \\ \dfrac{1}{R}\dfrac{\partial y}{\partial\theta} + \dfrac{1}{R^2}\dfrac{\partial^2 w_0}{\partial\theta^2} \\ \dfrac{\partial\phi_y}{\partial x} + \dfrac{1}{R}\dfrac{\partial\phi_x}{\partial\theta} + \dfrac{1}{R}\dfrac{\partial^2 w_0}{\partial x\partial\theta} \end{Bmatrix} \tag{16}$$

$$\boldsymbol{\gamma}_0 = \begin{Bmatrix} \phi_y + \dfrac{1}{R}\dfrac{\partial w_0}{\partial\theta} \\ \phi_x + \dfrac{\partial w_0}{\partial x} \end{Bmatrix}, \quad \boldsymbol{\gamma}_1 = -c_2\begin{Bmatrix} \phi_y + \dfrac{1}{R}\dfrac{\partial w_0}{\partial\theta} \\ \phi_x + \dfrac{\partial w_0}{\partial x} \end{Bmatrix} \tag{17}$$

where

$$c_2 = 3c_1 \quad \text{and} \quad c_1 = 4/3h^2 \tag{18}$$

Then, we can calculate the stress resultants as

$$\begin{Bmatrix} \mathbf{N}_0 \\ \mathbf{M}_0 \\ \mathbf{P}_0 \end{Bmatrix} = \begin{bmatrix} \mathbf{A}_0 & \mathbf{B}_0 & \mathbf{E}_0 \\ \mathbf{B}_0 & \mathbf{D}_0 & \mathbf{F}_0 \\ \mathbf{E}_0 & \mathbf{F}_0 & \mathbf{H}_0 \end{bmatrix}\begin{Bmatrix} \boldsymbol{\epsilon}_0 \\ \boldsymbol{\kappa}_2 \\ \boldsymbol{\kappa}_3 \end{Bmatrix} + \begin{Bmatrix} \mathbf{N}_T \\ \mathbf{M}_T \\ \mathbf{P}_T \end{Bmatrix} \tag{19}$$

$$\begin{Bmatrix} \mathbf{Q}_0 \\ \mathbf{R}_0 \end{Bmatrix} = \begin{bmatrix} \mathbf{A}_1 & \mathbf{D}_1 \\ \mathbf{D}_1 & \mathbf{F}_1 \end{bmatrix}\begin{Bmatrix} \boldsymbol{\gamma}_0 \\ \boldsymbol{\gamma}_2 \end{Bmatrix} \tag{20}$$

where the matrices $\mathbf{A}_0$, $\mathbf{B}_0$, $\mathbf{D}_0$, $\mathbf{E}_0$, $\mathbf{F}_0$, $\mathbf{H}_0$, $\mathbf{A}_1$, $\mathbf{D}_1$, $\mathbf{F}_1$, $\mathbf{N}_T$, $\mathbf{M}_T$ and $\mathbf{P}_T$ are given as

$$(\mathbf{A}_0, \mathbf{B}_0, \mathbf{D}_0, \mathbf{E}_0, \mathbf{F}_0, \mathbf{H}_0) = \int_{-h/2}^{h/2} \widehat{\mathbf{Q}}_b(\zeta)(1, \zeta, \zeta^2, \zeta^3, \zeta^4, \zeta^6)\, d\zeta \quad (21)$$

$$(\mathbf{A}_0, \mathbf{B}_0, \mathbf{D}_0, \mathbf{E}_0, \mathbf{F}_0, \mathbf{H}_0) = \int_{-h/2}^{h/2} \widehat{\mathbf{Q}}_b(\zeta)(1, \zeta, \zeta^2, \zeta^3, \zeta^4, \zeta^6)\, d\zeta \quad (22)$$

$$(\mathbf{N}_T, \mathbf{M}_T, \mathbf{P}_T) = \int_{-h/2}^{h/2} \widehat{\mathbf{Q}}_b(\zeta)\boldsymbol{\alpha}_0(1, \zeta, \zeta^3)d\zeta \quad (23)$$

where

$$\widehat{\mathbf{Q}}_b(\zeta) = \begin{bmatrix} \frac{E_{11}}{1-\upsilon_{12}\upsilon_{21}} & \frac{\upsilon_{21}E_{11}}{1-\upsilon_{12}\upsilon_{21}} & 0 \\ \frac{\upsilon_{21}E_{11}}{1-\upsilon_{12}\upsilon_{21}} & \frac{E_{11}}{1-\upsilon_{12}\upsilon_{21}} & 0 \\ 0 & 0 & G_{12} \end{bmatrix} \quad (24)$$

$$\widehat{\mathbf{Q}}_s(\zeta) = \begin{bmatrix} G_{23} & 0 \\ 0 & G_{13} \end{bmatrix}, \boldsymbol{\alpha}_0 = \begin{Bmatrix} \alpha_{11} \\ \alpha_{22} \\ 0 \end{Bmatrix} \quad (25)$$

Based on the Hamilton's principle of Li *et al*. (2009), the equation of motion of GRC-FG cylindrical shells is expressed as

$$\int_0^t [\delta(T - \Pi + W)]dt = 0 \quad (26)$$

where *T*, *U*, *W* are the kinetic energy, potential energy and work of the external loads which are given as

$$T = \frac{1}{2}\int \rho(\zeta)(\dot{u}^2 + \dot{v}^2 + \dot{w}^2)dV \quad (27)$$

$$U = \frac{1}{2}\int (\mathbf{N}_0^T\boldsymbol{\varepsilon}_0 + \mathbf{M}_0^T\boldsymbol{\kappa}_1 + \mathbf{P}_0^T\boldsymbol{\kappa}_3 + \mathbf{Q}_0^T\boldsymbol{\gamma}_0 + \mathbf{R}_0^T\boldsymbol{\gamma}_2)dA \quad (28)$$

$$W = -\frac{R}{2}\int \left[F_{Tx}\left(\frac{\partial w}{\partial x}\right)^2 + F_{T\theta}\left(\frac{\partial w}{R\partial\theta}\right)^2 + 2F_{Tx\theta}\frac{\partial w}{\partial x}\frac{\partial w}{R\partial\theta}\right]dxd\theta + k_1\lambda(t)w|_{(x_0,\theta_0)} + k_2\int \lambda(t)wdA \quad (29)$$

where *A* and *V* are the surface area and volume of the GRC-FG cylindrical shells, (F_{Tx}, F_{Tq}, F_{Txq}) are the in-plane thermal load, k_1 and k_2 are the thermal coefficients, and $\lambda(t)$ is the external load. In the present study, the assumed mode method (AMM) is applied to formulate the equation of motion for the GRC-FG cylindrical shells. Then the displacement fields of the GRC-FG cylindrical shells can be written as

$$u(x, \theta, t) = \sum_{i=1}^{m}\sum_{j=1}^{n} \phi_{ij}(x, \theta)p_{ij}(t) = \boldsymbol{\varphi}^T(x, \theta)\mathbf{p}(t) \quad (30)$$

$$v(x, \theta, t) = \sum_{i=1}^{m}\sum_{j=1}^{n} \psi_{ij}(x, \theta)q_{ij}(t) = \boldsymbol{\psi}^T(x, \theta)\mathbf{q}(t) \quad (31)$$

$$w(x, \theta, t) = \sum_{i=1}^{m}\sum_{j=1}^{n} \varpi_{ij}(x, \theta)r_{ij}(t) = \boldsymbol{\varpi}^T(x, \theta)\mathbf{r}(t) \quad (32)$$

$$\phi_x(x, \theta, t) = \sum_{i=1}^{m}\sum_{j=1}^{n} \vartheta_{ij}(x, \theta)f_{ij}(t) = \boldsymbol{\vartheta}^T(x, \theta)\mathbf{f}(t) \quad (33)$$

$$\phi_y(x, \theta, t) = \sum_{i=1}^{m}\sum_{j=1}^{n} \xi_{ij}(x, \theta)g_{ij}(t) = \boldsymbol{\xi}^T(x, \theta)\mathbf{g}(t) \quad (34)$$

where ($\boldsymbol{\varphi}$, $\boldsymbol{\psi}$, $\boldsymbol{\varpi}$, $\boldsymbol{\vartheta}$, $\boldsymbol{\xi}$) are the column vectors of the assumed mode and (**p**, **q**, **r**, **f**, **g**) are the generalized coordinate vectors. *m* and *n* are the mode numbers in the *x* and θ directions.

By substituting the Eqs. (10)-(12), (13)-(17), (19)-(20) and (30)-(34) into Eq. (13), and the results into Eq. (26), we can obtain the equation of motion by taking the variation calculations as follow

$$\mathbf{M}\ddot{\mathbf{X}}(t) + (\mathbf{K} + \mathbf{K}_{\Delta T})\mathbf{X}(t) = k_1\lambda(t)\mathbf{F}_c + k_2\lambda(t)\mathbf{F}_d \quad (35)$$

where $\mathbf{X}(t) = (\mathbf{p}(t)^T, \mathbf{q}(t)^T, \mathbf{r}(t)^T, \mathbf{f}(t)^T, \mathbf{g}(t)^T)$ is the generalized coordinate vector. **M**, **K**, $\mathbf{K}_{\Delta T}$, $\mathbf{F}_c$ and $\mathbf{F}_d$ are the modal mass, stiffness matrices, the thermal stiffness matrix and the force vectors, which can be calculated as follow

$$\mathbf{M} = \begin{bmatrix} \mathbf{M}_{uu} & 0 & \mathbf{M}_{uw} & \mathbf{M}_{ux} & 0 \\ 0 & \mathbf{M}_{vv} & \mathbf{M}_{vw} & 0 & \mathbf{M}_{v\theta} \\ \mathbf{M}_{uw}^T & \mathbf{M}_{vw}^T & \mathbf{M}_{ww} & \mathbf{M}_{wx} & \mathbf{M}_{w\theta} \\ \mathbf{M}_{ux}^T & 0 & \mathbf{M}_{wx}^T & \mathbf{M}_{xx} & 0 \\ 0 & \mathbf{M}_{v\theta}^T & \mathbf{M}_{w\theta}^T & 0 & \mathbf{M}_{\theta\theta} \end{bmatrix}_{5m_0\times 5m_0} \quad (36)$$

$$\mathbf{K} = \begin{bmatrix} \mathbf{K}_{uu} & \mathbf{K}_{uv} & \mathbf{K}_{uw} & \mathbf{K}_{ux} & \mathbf{K}_{u\theta} \\ \mathbf{K}_{uv}^T & \mathbf{K}_{vv} & \mathbf{K}_{vw} & \mathbf{K}_{vx} & \mathbf{K}_{v\theta} \\ \mathbf{K}_{uw}^T & \mathbf{K}_{vw}^T & \mathbf{K}_{ww} & \mathbf{K}_{wx} & \mathbf{K}_{w\theta} \\ \mathbf{K}_{ux}^T & \mathbf{K}_{vx}^T & \mathbf{K}_{wx}^T & \mathbf{K}_{xx} & \mathbf{K}_{x\theta} \\ \mathbf{K}_{u\theta}^T & \mathbf{K}_{v\theta}^T & \mathbf{K}_{w\theta}^T & \mathbf{K}_{x\theta}^T & \mathbf{K}_{\theta\theta} \end{bmatrix}_{5m_0\times 5m_0} \quad (37)$$

$$\mathbf{K}_{\Delta T} = \begin{bmatrix} 0 & 0 & 0 & 0 & 0 \\ 0 & 0 & 0 & 0 & 0 \\ 0 & 0 & \mathbf{K}_{ww}^{\Delta T} & 0 & 0 \\ 0 & 0 & 0 & 0 & 0 \\ 0 & 0 & 0 & 0 & 0 \end{bmatrix}_{5m_0\times 5m_0} \quad (38)$$

$$\mathbf{F}_c = [0 \quad 0 \quad \varpi^T(x_0, \theta_0) \quad 0 \quad 0]_{5m_0\times 1}^T \quad (39)$$

$$\mathbf{F}_d = \left[0 \quad 0 \quad \int \varpi^T dA \quad 0 \quad 0\right]_{5m_0\times 1}^T \quad (40)$$

where (x_0, θ_0) is the point where the concentrated forced is applied, $m_0 = m\times n$, and, the components of the mass and stiffness matrix are presented in appendix A.

For above equations, coefficients m_{uu}, m_{uw}, m_{ux}, m_{vv}, m_{vw}, $m_{v\theta}$, m_{ww1}, m_{ww2}, m_{ww3}, m_{wx}, $m_{w\theta}$, m_{xx}, and $m_{\theta\theta}$ can be calculated based on the distributions of graphene. For FGX-GRC-FG cylindrical shells, these coefficients are given in appendix B.

We assume $\mathbf{X}(t) = \mathbf{X}_0 e\omega t$ as the general solution of homogeneous differential equation of Eq. (15), in which $\mathbf{X}_0$ and ω are the eigenvector and eigenvalue. Substituting $\mathbf{X}(t) = \mathbf{X}_0 e\omega t$ into the homogeneous differential equation of Eq. (15), and the natural frequency of the GRC-FG cylindrical shells can be derived by letting the coefficient determinant to be zero.

For free vibration responses (k_1 = 1 and k_2 = 0) of the GRC-FG cylindrical shells, through the function ode45 or impulse of MATLAB software, the free vibration responses (k_1 = 1 and k_2 = 0) of the GRC-FG cylindrical shells can be obtained. For the forced vibration responses (k_1 = 0 and k_2 = 1) of the GRC-FG cylindrical shells, the distributed external load in the transverse direction is given as

$$\lambda(x,\theta,t) = \lambda_1 \sin\Omega t + \lambda_2 \cos\Omega t \tag{41}$$

where λ_1, λ_2 and Ω are the amplitude and frequency of the dynamic load. The steady-state solution of Eq. (15) under the external dynamic load can be expressed as

$$\mathbf{X}(t) = \mathbf{\Pi}_1 \sin\Omega t + \mathbf{\Pi}_1 \cos\Omega t \tag{42}$$

where $\mathbf{\Pi}_1$ and $\mathbf{\Pi}_2$ are the amplitude values of forced vibration responses (k_1 = 0 and k_2 = 1) of the GRC-FG cylindrical shells. Substituting Eqs. (19) and (20) into Eq. (15), we can obtain the following equation

$$\begin{bmatrix} \mathbf{K}+\mathbf{K}_{\Delta T}-\Omega^2\mathbf{M} & 0 \\ 0 & \mathbf{K}+\mathbf{K}_{\Delta T}-\Omega^2\mathbf{M} \end{bmatrix} \begin{Bmatrix} \mathbf{\Pi}_1 \\ \mathbf{\Pi}_1 \end{Bmatrix} = \begin{Bmatrix} \lambda_1 \mathbf{F}_d \\ \lambda_2 \mathbf{F}_d \end{Bmatrix} \tag{43}$$

from which the forced vibration amplitude $\mathbf{\Pi}_1$ and $\mathbf{\Pi}_2$ can be obtained.

For the present GRC-FG cylindrical shells, the boundary conditions are simply supported on its two ends. Therefore, modes satisfying the simply supported boundary conditions are assumed as

$$\varphi_{ij} = \vartheta_{ij} = \cos\frac{i\pi x}{L}\cos j\theta \tag{44}$$

$$\psi_{ij} = \xi_{ij} = \sin\frac{i\pi x}{L}\sin j\theta \tag{45}$$

Table 1 Material properties for monolayer graphene in different temperature environments of Shen *et al*. (2018)

T	E_{11}^G (Gpa)	E_{22}^G (GPa)	G_{12}^G (Gpa)	α_{11}^G (/K)	α_{22}^G (/K)
300	1812	1807	683	-0.90×10^{-6}	-0.95×10^{-6}
400	1769	1763	691	-0.35×10^{-6}	-0.40×10^{-6}
500	1748	1735	700	-0.08×10^{-6}	-0.08×10^{-6}

$$\varpi_{ij} = \sin\frac{i\pi x}{L}\cos j\theta \tag{46}$$

4. Numerical results and discussion

In this section, detailed parametric studies are conducted for free and force vibration of the GRC-FG cylindrical shells. The zigzag graphene sheets with properties a_G = 14.76 nm, b_G = 14.77 nm, h_G = 0.188 nm, r_G = 4118 kg/m^{3}and u_{12}^G = 0.11 are selected as reinforcements. The material properties of zigzag graphene sheets in different temperature environments are given in Table 1.

Poly (methyl methacrylate), referred to as PMMA, is selected for the matrix with the material properties r_m = 1150 kg/m^3, v^m = 0.34 and E^m = (3.52 – 0.0034T) GPa, in which $T = T_0 + \Delta T$ and T_0 = 300K. The graphene efficiency parameters η_j (j = 1, 2, 3) for different volume fractions the GRC-FG cylindrical shells in different temperature environments are obtained by matching the material properties of GRCs predicted from the Halpin-Tsai model to those from the MD simulations of Shen *et al*. (2018), which are listed in Table 2.

Firstly, the accuracy of the proposed method was verified through the comparison study. Isotropic cylindrical shell with L = 0.41 m, R = 0.3015 m, h = 0.001 m, r = 7850 kg/m^3, v = 0.3 and E = 210 GPa are considered. Table 3 shows the natural frequencies of the isotropic cylindrical shell with m = 1 and n changing from 7 to 15. It is obviously seen that the present natural frequencies agree well with those in the literature of Dym (1973), Gasser (1987), Shen and Xiang (2012) which indicates that the method used in this study is accurate and effective.

A further convergence study is carried out for free vibration for UD GRC-FG cylindrical shell. Fig. 2 shows

Table 2 Efficiency parameters for different volume fractions GRC-FG plates in different temperature environments of Shen *et al*. (2018)

T	V_G	h_1	h_2	h_3
300 K	0.03	2.929	2.855	11.842
	0.05	3.068	2.962	15.944
	0.07	3.013	2.966	23.575
	0.09	2.647	2.609	32.816
	0.11	2.311	2.260	33.125
400 K	0.03	2.978	2.867	13.929
	0.05	3.129	3.024	15.230
	0.07	3.061	3.028	22.589
	0.09	2.702	2.604	28.870
	0.11	2.406	2.338	29.528
500 K	0.03	3.389	3.383	16.713
	0.05	3.545	3.415	16.019
	0.07	3.463	3.340	23.429
	0.09	3.059	2.937	29.755
	0.11	2.737	2.666	30.774

Table 3 Comparison of natural frequencies (Hz) for the isotropic cylindrical shell with different values of assumed mode n

n	Present	Gasser (1987)	Shen and Xiang (2012)	Dym (1973)
7	303.3358	318	306.73	305.32
8	280.9185	278	283.30	281.37
9	288.6769	290	290.59	288.28
10	318.3476	334	320.04	317.51
11	363.2488	362	364.83	362.22
12	419.0646	418	420.59	417.96
13	476.9604	478	484.84	482.23
14	554.7735	550	556.24	553.67
15	632.6257	626	634.08	631.59

the free vibration responses for UD GRC-FG cylindrical shell with (m = 8, n = 8) and (m = 13, n = 13). It is evident that there is a large difference between the free vibration responses of the UD GRC-FG cylindrical shell computed by (m = 8, n = 8) and (m = 13, n = 13). Fig. 3 presents free vibration responses for UD GRC-FG cylindrical shell with (m = 13, n = 13) and m = 15, n = 15. It can be seen that the free vibration responses of UD GRC-FG cylindrical shell with (m = 13, n = 13) and (m = 15, n = 15) are almost the same. Therefore, in the following cases, unless otherwise stated, (m = 13, n = 13) are used for the free and force

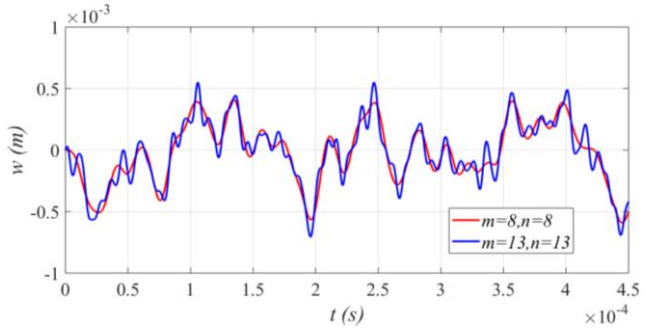

Fig. 2 Free vibration responses for UD GRC-FG cylindrical shell with (m = 8, n = 8) and (m = 13, n = 13)

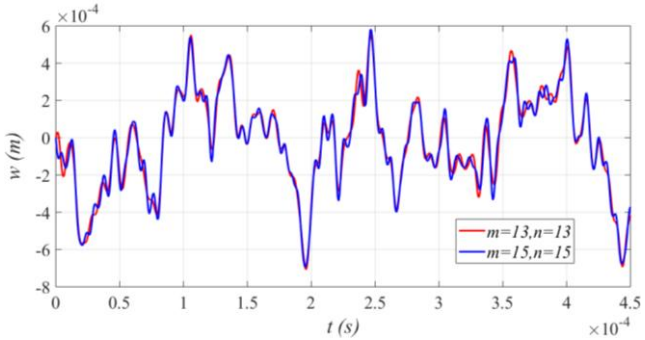

Fig. 3 Free vibration responses for UD GRC-FG cylindrical shell with (m = 13, n = 13) and (m = 15, n = 15)

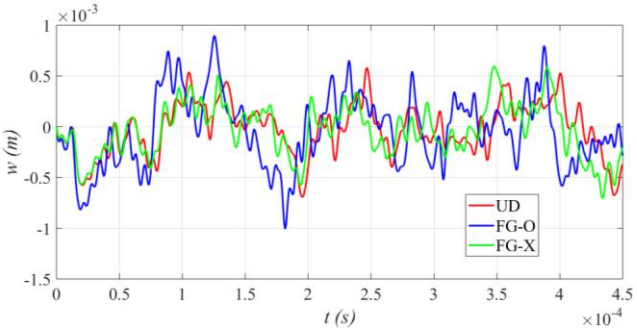

Fig. 4 Free vibration responses for various types of GRC-FG cylindrical shells

vibration of the GRC-FG cylindrical shells.

Fig. 4 depicts the free vibration responses for UD, FG-O and FG-X of GRC-FG cylindrical shells. It is seen from the figure that the free vibration amplitude of FG-O GRC-FG cylindrical shell is higher than that of FG-X GRC-FG cylindrical shell while the free vibration amplitude of UD GRC-FG cylindrical shell is higher than the frequency of FG-X GRC-FG cylindrical shell. Therefore, it can be concluded that the strengthening of the stiffness near the surfaces of GRC-FG cylindrical shells is more effective in reducing the vibration amplitude of the cylindrical shell structure.

Therefore, stiffness of the GRC-FG cylindrical shells can be designed by using different distributions of graphene in the composite, and the vibration frequencies and vibration amplitudes can be also devised by the distributions of graphene. In other words, suitable distribution of graphene can suppress the vibration of the shell. From the view of passive vibration control, changing distribution is effective. This can be helpful of some practical application requirement.

For the UD GRC-FG cylindrical shells with different value of shell radius-to-thickness ratio R/h, the free vibration responses are shown in Fig. 5. It can be seen that with the GRC-FG cylindrical shells become relatively large, the free vibration amplitude become higher. That is obvious because large cylindrical shells are easier to deform. For FG-O and FG-X of GRC-FG cylindrical shells with different value of shell radius-to-thickness ratio R/h, the

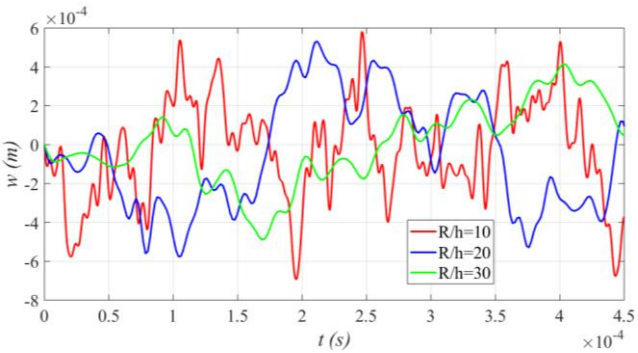

Fig. 5 Free vibration responses for UD GRC-FG cylindrical shells with different value of R/h

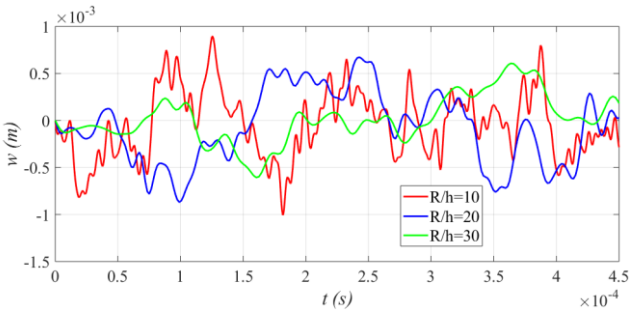

Fig. 6 Free vibration responses for FG-O GRC-FG cylindrical shells with different value of R/h

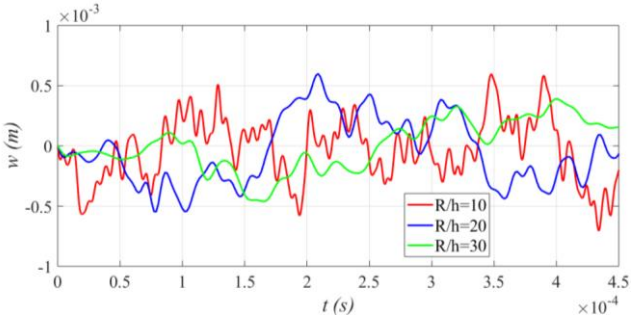

Fig. 7 Free vibration responses for FG-X GRC-FG cylindrical shells with different value of R/h

free vibration responses are shown in Figs. 6 and 7. Similar change trend is also obtained for of radius-to-thickness ratio R/h for FG-O and FG-X GRC-FG cylindrical shells. As the stiffness and vibration responses are significantly affect by the geometry of GRC-FG cylindrical shells, we can choose suitable size GRC-FG cylindrical shells to design the stiffness and vibration properties of the resulting nanocomposites.

Fig. 8 shows the free vibration responses for UD GRC-FG cylindrical shells in different temperature environments. It can be seen that with the temperature environments changing from 300 K to 500 K, the free vibration amplitude of UD GRC-FG cylindrical shells increases. That because the material properties of the resulting GRC-FG cylindrical shells decrease when the temperature increases. Figs. 9 and 10 present the corresponding free vibration responses for

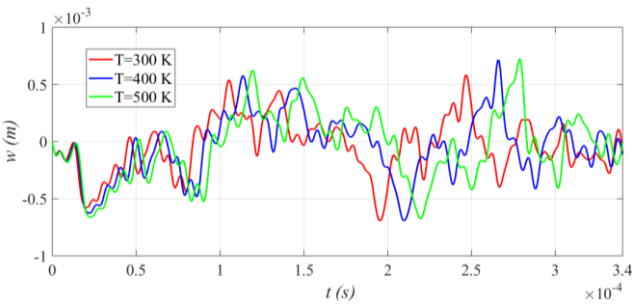

Fig. 8 Free vibration responses for UD GRC-FG cylindrical shells in different temperature environments

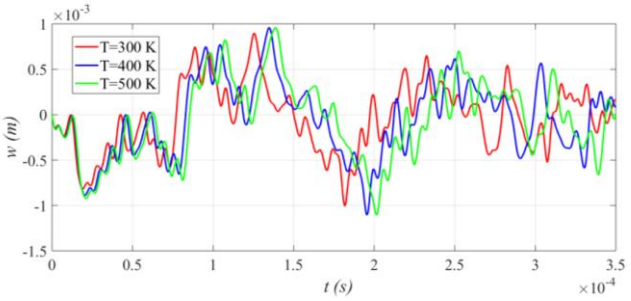

Fig. 9 Free vibration responses for FG-O GRC-FG cylindrical shells in different temperature environments

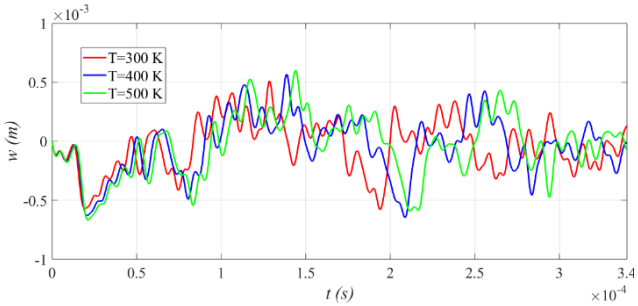

Fig. 10 Free vibration responses for FG-X GRC-FG cylindrical shells with different value of R/h

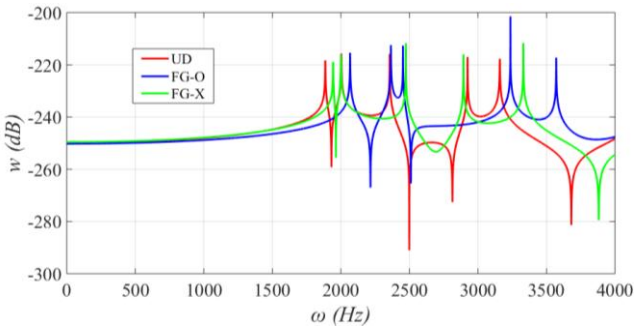

Fig. 11 Forced vibration responses for various types of GRC-FG cylindrical shells

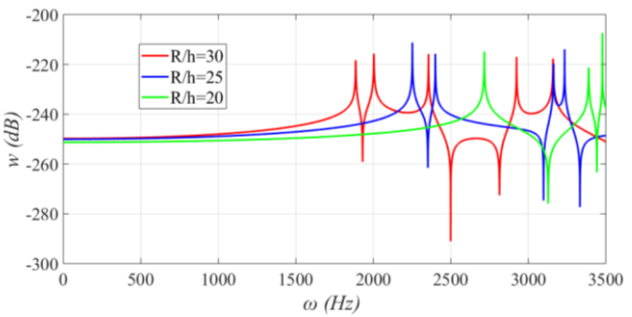

Fig. 12 Forced vibration responses for UD GRC-FG cylindrical shells with different value of R/h

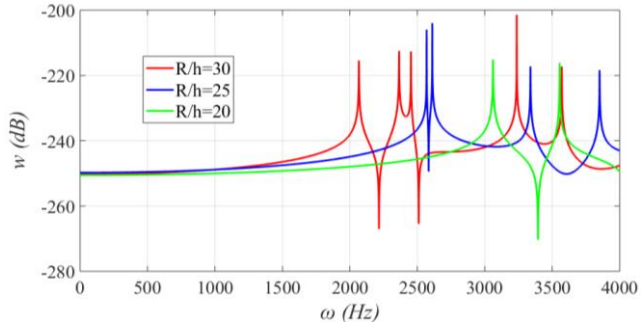

Fig. 13 Forced vibration responses for FG-O GRC-FG cylindrical shells with different value of R/h

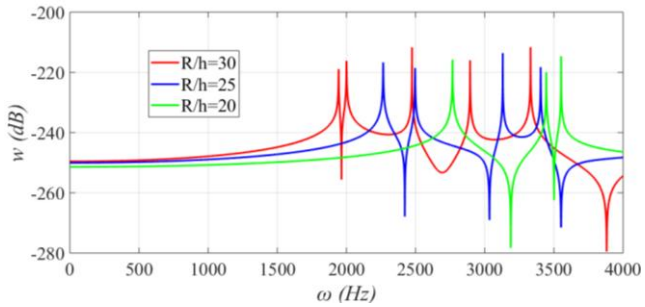

Fig. 14 Forced vibration responses for FG-X GRC-FG cylindrical shells with different value of R/h

FG-O and FG-X GRC-FG cylindrical shells in different temperature environments.

Fig. 11 shows the forced vibration responses for various types of GRC-FG cylindrical shells. It can be seen that for the forced vibration responses for various types of GRC-FG cylindrical shells, the forced vibration amplitude is largest for FG-O GRC-FG cylindrical shells, lowest for FG-X GRC-FG cylindrical shells. Then we can reach the same conclusion for the distribution of graphene for the forced vibration compared with the conclusion of free vibration.

Figs. 12-14 presents the forced vibration responses for UD, FG-O and FG-X GRC-FG cylindrical shells with different value of shell radius-to-thickness ratio R/h. It can be seen that with the decrease of shell radius-to-thickness ratio R/h, the forced vibration amplitudes for UD, FG-O and FG-X GRC-FG cylindrical shells decrease.

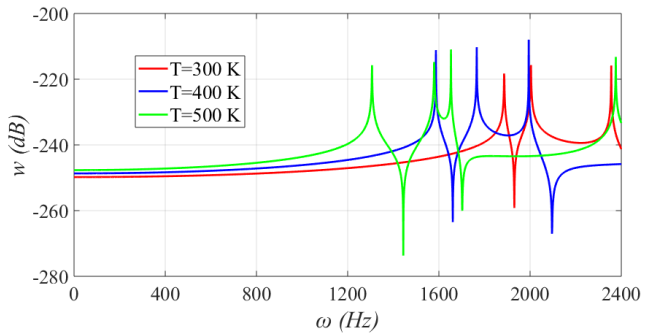

Fig. 15 Forced vibration responses for UD GRC-FG cylindrical shells in different temperature environments

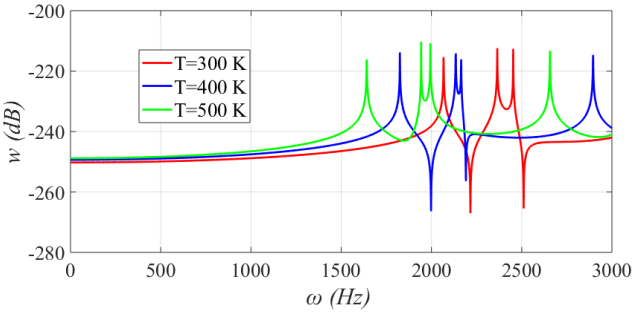

Fig. 16 Forced vibration responses for FG-O GRC-FG cylindrical shells in different temperature environments

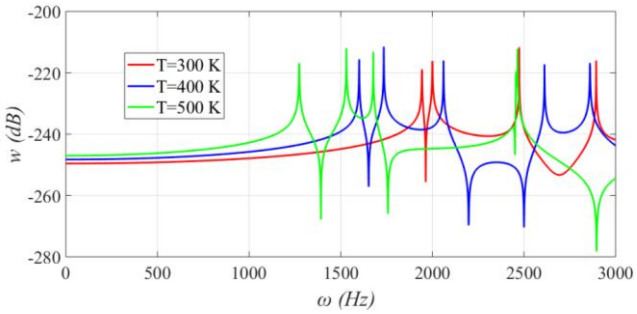

Fig. 17 Forced vibration responses for FG-X GRC-FG cylindrical shells in different temperature environments

Figs. 15-17 presents the forced vibration responses for UD, FG-O and FG-X GRC-FG cylindrical shells in different temperature environments. As it is expected, with the increase of the temperature, the force vibration amplitude of the shell UD, FG-O and FG-X GRC-FG cylindrical shells increases. From these figures, we can also find that with the increase of the temperature, the frequencies of the UD, FG-O and FG-X GRC-FG cylindrical shells increases. As shown in Fig.1, the material properties of graphene decrease with the increase of temperature, also the material properties of matrix decrease.

Therefore, the resulting material properties of the GRC-FG cylindrical shells which lead lower stiffness in higher temperature. Then GRC-FG cylindrical shells deform largely in higher temperature environment.

5. Conclusions

In this paper, the time- and frequency-domain methods are implemented for free and force vibration behaviors of graphene-reinforced composite functionally graded (GRC-FG) cylindrical shells in thermal environments based on Reddy's third-order shear deformation theory (HSDT). The GRC-FG cylindrical shells are composed of piece-wise pattern graphene-reinforced layers which have different volume fraction. Based on the extended Halpin-Tsai micromechanical model, the effective material properties of the resulting nanocomposites are evaluated. Using the Hamilton's principle and the assumed mode method, the

motion equation of the GRC-FG cylindrical shells is formulated. Numerical examples are presented to investigate the effects of distribution of graphene, shell radius-to-thickness ratio and temperature changes on the free and force vibration responses of GRC-FG cylindrical shells. Some typical conclusions are obtained as follow:

(a) The strengthening of the stiffness near the surfaces of GRC-FG cylindrical shells is more effective in reducing the vibration amplitude of the cylindrical shell structure. Therefore, suitable distribution of graphene can suppress the vibration of the shell.
(b) The stiffness and vibration responses are significantly affected by the geometry of GRC-FG cylindrical shells. We can choose suitable size GRC-FG cylindrical shells to design the stiffness and vibration properties of the resulting nanocomposites.
(c) Temperature increase will lead decrease of the free and force vibration responses of GRC-FG cylindrical shells.

Acknowledgments

The work described in this paper was fully supported by the National Natural Science Foundation of China (Grant no. 11702138).

References

Ansari, R., Torabi, J. and Shojaei, M.F. (2017), "Buckling and vibration analysis of embedded functionally graded carbon nanotube-reinforced composite annular sector plates under thermal loading", *Compos. Part B*: *Eng.*, **109**, 197-213. https://doi.org/10.1016/j.compositesb.2016.10.050

Arani, A.G., Kolahdouzan, F. and Abdollahian, M. (2018), "Buckling and free vibration analysis of FG-CNTRC-micro sandwich plate", *Steel Compos. Struct., Int. J.*, **26**(3), 273-287. https://doi.org/10.12989/scs.2018.26.3.273

Asadi, H. (2017), "Numerical simulation of the fluid-solid interaction for CNT reinforced functionally graded cylindrical shells in thermal environments", *Acta Astronautica*, **138**, 214-224. https://doi.org/10.1016/j.actaastro.2017.05.039

Asadi, H. and Beheshti, A.R. (2018), "On the nonlinear dynamic responses of FG-CNTRC beams exposed to aerothermal loads using third-order piston theory", *Acta Mechanica*, **229**(6), 2413-2430. https://doi.org/10.1007/s00707-018-2121-7

Asadi, H. and Wang, Q. (2017a), "Dynamic stability analysis of a pressurized FG-CNTRC cylindrical shell interacting with supersonic airflow", *Compos. Part B*: *Eng.*, **118**, 15-25. https://doi.org/10.1016/j.compositesb.2017.03.001

Asadi, H. and Wang, Q. (2017b), "An investigation on the aeroelastic flutter characteristics of FG-CNTRC beams in the supersonic flow", *Compos. Part B*: *Eng.*, **116**, 486-499. https://doi.org/10.1016/j.compositesb.2016.10.089

Asadi, H., Souri, M. and Wang, Q. (2017), "A numerical study on flow-induced instabilities of supersonic FG-CNT reinforced composite flat panels in thermal environments", *Compos. Struct.*, **171** 113-125. https://doi.org/10.1016/j.compstruct.2017.02.003

Bahrami, M.N., Allahkarami, F. and Saryazdi, M.G. (2018), "Nonlinear forced vibration of FG-CNTs-reinforced curved microbeam based on strain gradient theory considering out-of-plane motion", *Steel Compos. Struct., Int. J.*, **26**(6), 673-691. https://doi.org/10.12989/scs.2018.26.6.673

Chu, K., Wang, X.-h., Li, Y.-b., Huang, D.-j., Geng, Z.-r., Zhao, X.-l., Liu, H. and Zhang, H. (2018), "Thermal properties of graphene/metal composites with aligned graphene", *Mater. Des.*, **140**, 85-94. https://doi.org/10.1016/j.matdes.2017.11.048

Dym, C.L. (1973), "Some new results for the vibrations of circular cylinders", *J. Sound Vib.*, **29**(2), 189-205. https://doi.org/10.1016/S0022-460X(73)80134-8

Fantuzzi, N., Tornabene, F., Bacciocchi, M. and Dimitri, R. (2017), "Free vibration analysis of arbitrarily shaped Functionally Graded Carbon Nanotube-reinforced plates", *Compos. Part B*: *Eng.*, **115**, 384-408. https://doi.org/10.1016/j.compositesb.2016.09.021

Feng, C., Kitipornchai, S. and Yang, J. (2017), "Nonlinear bending of polymer nanocomposite beams reinforced with non-uniformly distributed graphene platelets (GPLs)", *Compos. Part B*: *Eng.*, **110**, 132-140. https://doi.org/10.1016/j.compositesb.2016.11.024

Gasser, L.F.F. (1987), "Free vibrations of thin cylindrical shells containing liquid", M.S. Thesis; Federal University of Rio de Janeiro, PEC·COPPE-UFRJ, Rio de Janeiro, Brazil. [In Portuguese]

Gong, S.W., Toh, S.L. and Shim, V.P.W. (1994), "The elastic response of orthotropic laminated cylindrical shells to low-velocity impact", *Compos. Eng.*, **4**(2), 247-266. https://doi.org/10.1016/0961-9526(94)90030-2

Gul, U. and Aydogdu, M. (2018), "Noncoaxial vibration and buckling analysis of embedded double-walled carbon nanotubes by using doublet mechanics", *Compos. Part B*: *Eng.*, **137**, 60-73. https://doi.org/10.1016/j.compositesb.2017.11.005

Harbaoui, I., Casimir, J.B., Khadimallah, M.A. and Chafra, M. (2018), "A new prestressed dynamic stiffness element for vibration analysis of thick circular cylindrical shells", *Int. J. Mech. Sci.*, **140**, 37-50. https://doi.org/10.1016/j.ijmecsci.2018.02.046

Hosseini, S.M. and Zhang, C. (2018), "Elastodynamic and wave propagation analysis in a FG graphene platelets-reinforced nanocomposite cylinder using a modified nonlinear micromechanical model", *Steel Compos. Struct., Int. J.*, **27**(3), 255-271. https://doi.org/10.12989/scs.2018.27.3.255

Jensen, B.D., Odegard, G.M., Kim, J.-W., Sauti, G., Siochi, E.J. and Wise, K.E. (2018), "Simulating the effects of carbon nanotube continuity and interfacial bonding on composite strength and stiffness", *Compos. Sci. Technol.*, **166**, 10-19. https://doi.org/10.1016/j.compscitech.2018.02.008

Keleshteri, M.M., Asadi, H. and Wang, Q. (2017a), "Large amplitude vibration of FG-CNT reinforced composite annular plates with integrated piezoelectric layers on elastic foundation", *Thin-Wall. Struct.*, **120**, 203-214. https://doi.org/10.1016/j.tws.2017.08.035

Keleshteri, M.M., Asadi, H. and Wang, Q. (2017b), "Postbuckling analysis of smart FG-CNTRC annular sector plates with surface-bonded piezoelectric layers using generalized differential quadrature method", *Comput. Methods Appl. Mech. Eng.*, **325**, 689-710. https://doi.org/10.1016/j.cma.2017.11.015

Keleshteri, M.M., Asadi, H. and Wang, Q. (2018), "On the snap-through instability of post-buckled FG-CNTRC rectangular plates with integrated piezoelectric layers", *Comput. Methods Appl. Mech. Eng.*, **331**, 53-71. https://doi.org/10.1016/j.cma.2017.11.015

Keleshteri, M.M., Asadi, H. and Aghdam, M.M. (2019), "Nonlinear bending analysis of FG-CNTRC annular plates with variable thickness on elastic foundation", *Thin-Wall. Struct.*, **135**, 453-462. https://doi.org/10.1016/j.tws.2018.11.020

Kiani, Y. (2018), "Isogeometric large amplitude free vibration of

graphene reinforced laminated plates in thermal environment using NURBS formulation", *Comput. Methods Appl. Mech. Eng.*, **332**, 86-101. https://doi.org/10.1016/j.cma.2017.12.015

Kumar, P. and Srinivas, J. (2018), "Transient vibration analysis of FG-MWCNT reinforced composite plate resting on foundation", *Steel Compos. Struct., Int. J.*, **29**(5), 569-578. https://doi.org/10.12989/scs.2018.29.5.569

Lei, Z. and Zhang, Y. (2018), "Characterizing buckling behavior of matrix-cracked hybrid plates containing CNTR-FG layers", *Steel Compos. Struct., Int. J.*, **28**(4), 495-508. https://doi.org/10.12989/scs.2018.28.4.495

Lei, Z., Su, Q., Zeng, H., Zhang, Y. and Yu, C. (2018), "Parametric studies on buckling behavior of functionally graded graphene-reinforced composites laminated plates in thermal environment", *Compos. Struct.*, **202**, 695-709. https://doi.org/10.1016/j.compstruct.2018.03.079

Li, F.-M., Kishimoto, K. and Huang, W.-H. (2009), "The calculations of natural frequencies and forced vibration responses of conical shell using the Rayleigh–Ritz method", *Mech. Res. Commun.*, **36**(5), 595-602. https://doi.org/10.1016/j.mechrescom.2009.02.003

Liew, K.M., Zhao, X. and Lee, Y.Y. (2012), "Postbuckling responses of functionally graded cylindrical shells under axial compression and thermal loads", *Compos. Part B: Eng.*, **43**(3), 1621-1630. https://doi.org/10.1016/j.compositesb.2011.06.004

Liew, K.M., Lei, Z.X., Yu, J.L. and Zhang, L.W. (2014), "Postbuckling of carbon nanotube-reinforced functionally graded cylindrical panels under axial compression using a meshless approach", *Comput. Methods Appl. Mech. Eng.*, **268**, 1-17. https://doi.org/10.1016/j.cma.2013.09.001

Liew, K.M., Lei, Z.X. and Zhang, L.W. (2015), "Mechanical analysis of functionally graded carbon nanotube reinforced composites: A review", *Compos. Struct.*, **120**, 90-97. https://doi.org/10.1016/j.compstruct.2014.09.041

Mehri, M., Asadi, H. and Wang, Q. (2016a), "Buckling and vibration analysis of a pressurized CNT reinforced functionally graded truncated conical shell under an axial compression using HDQ method", *Comput. Methods Appl. Mech. Eng.*, **303**, 75-100. https://doi.org/10.1016/j.cma.2016.01.017

Mehri, M., Asadi, H. and Wang, Q. (2016b), "On dynamic instability of a pressurized functionally graded carbon nanotube reinforced truncated conical shell subjected to yawed supersonic airflow", *Compos. Struct.*, **153**, 938-951. https://doi.org/10.1016/j.compstruct.2016.07.009

Mehri, M., Asadi, H. and Kouchakzadeh, M.A. (2017), "Computationally efficient model for flow-induced instability of CNT reinforced functionally graded truncated conical curved panels subjected to axial compression", *Comput. Methods Appl. Mech. Eng.*, **318**, 957-980. https://doi.org/10.1016/j.cma.2017.02.020

Mohammadzadeh-Keleshteri, M., Asadi, H. and Aghdam, M.M. (2017), "Geometrical nonlinear free vibration responses of FG-CNT reinforced composite annular sector plates integrated with piezoelectric layers", *Compos. Struct.*, **171**, 100-112. https://doi.org/10.1016/j.compstruct.2017.01.048

Rafiee, M.A., Rafiee, J., Yu, Z.Z. and Koratkar, N. (2009), "Buckling resistant graphene nanocomposites", *Appl. Phys. Lett.*, **95**(22), 223103. https://doi.org/10.1063/1.3269637

Reddy, J.N. (1999), "On laminated composite plates with integrated sensors and actuators", *Eng. Struct.*, **21**(7), 568-593.

Shakouri, M. and Kouchakzadeh, M.A. (2017), "Analytical solution for vibration of generally laminated conical and cylindrical shells", *Int. J. Mech. Sci.*, **131-132**, 414-425. https://doi.org/10.1016/j.ijmecsci.2017.07.016

Shen, H.-S. and Xiang, Y. (2012), "Nonlinear vibration of nanotube-reinforced composite cylindrical shells in thermal environments", *Comput. Methods Appl. Mech. Eng.*, **213-216**, 196-205. https://doi.org/10.1016/j.cma.2011.11.025

Shen, H.-S., He, X.Q. and Yang, D.-Q. (2017), "Vibration of thermally postbuckled carbon nanotube-reinforced composite beams resting on elastic foundations", *Int. J. Non-Linear Mech.*, **91**, 69-75. https://doi.org/10.1016/j.ijnonlinmec.2017.02.010

Shen, H.-S., Xiang, Y., Fan, Y. and Hui, D. (2018), "Nonlinear vibration of functionally graded graphene-reinforced composite laminated cylindrical panels resting on elastic foundations in thermal environments", *Compos. Part B: Eng.*, **136**, 177-186. https://doi.org/10.1016/j.compositesb.2017.10.032

Sofiyev, A.H., Karaca, Z. and Zerin, Z. (2017), "Non-linear vibration of composite orthotropic cylindrical shells on the non-linear elastic foundations within the shear deformation theory", *Compos. Struct.*, **159**, 53-62. https://doi.org/10.1016/j.compstruct.2016.09.048

Song, Z.G., Zhang, L.W. and Liew, K.M. (2016a), "Active vibration control of CNT reinforced functionally graded plates based on a higher-order shear deformation theory", *Int. J. Mech. Sci.*, **105**, 90-101. https://doi.org/10.1016/j.ijmecsci.2015.11.019

Song, Z.G., Zhang, L.W. and Liew, K.M. (2016b), "Dynamic responses of CNT reinforced composite plates subjected to impact loading", *Compos. Part B: Eng.*, **99**, 154-161. https://doi.org/10.1016/j.compositesb.2016.06.034

Tahouneh, V. (2018), "Vibration analysis of sandwich sectorial plates considering FG wavy CNT-reinforced face sheets", *Steel Compos. Struct., Int. J.*, **28**(5), 541-557. https://doi.org/10.12989/scs.2018.28.5.541

Tornabene, F., Arefi, M., Mohammadi, M., Tabatabaeian, A. and Dimitri, R. (2018), "Two-dimensional thermo-elastic analysis of FG-CNTRC cylindrical pressure vessels", *Steel Compos. Struct, Int. J.*, **27**(4), 525-536. https://doi.org/10.12989/scs.2018.27.4.525

Vertuccio, L., Guadagno, L., Spinelli, G., Russo, S. and Iannuzzo, G. (2017), "Effect of carbon nanotube and functionalized liquid rubber on mechanical and electrical properties of epoxy adhesives for aircraft structures", *Compos. Part B: Eng.*, **129**, 1-10. https://doi.org/10.1016/j.compositesb.2017.07.021

Wan, X., Fan, Y., Ma, W., Li, S., Huang, X. and Yu, J. (2018), "One-step synthesis of nano-silicon/graphene composites using thermal plasma approach", *Mater. Lett.*, **220**, 144-147. https://doi.org/10.1016/j.matlet.2018.03.042

Yang, J., Wu, H. and Kitipornchai, S. (2018), "Free vibration of thermo-electro-mechanically postbuckled FG-CNTRC beams with geometric imperfections", *Steel Compos. Struct., Int. J.*, **29**(3), 319-332. https://doi.org/10.12989/scs.2018.29.3.319

Zhan, J.M., Yao, X.H., Li, W.H. and Zhang, X.Q. (2017), "Tensile mechanical properties study of SiC/graphene composites based on molecular dynamics", *Computat. Mater. Sci.*, **131**, 266-274. https://doi.org/10.1016/j.commatsci.2017.02.006

Zhang, X.M., Liu, G.R. and Lam, K.Y. (2001), "Vibration analysis of thin cylindrical shells using wave propagation approach", *J. Sound Vib.*, **239**(3), 397-403. https://doi.org/10.1006/jsvi.2000.3139

Zhang, W., Fang, Z., Yang, X.-D. and Liang, F. (2018), "A series solution for free vibration of moderately thick cylindrical shell with general boundary conditions", *Eng. Struct.*, **165**, 422-440. https://doi.org/10.1016/j.engstruct.2018.03.049

CC

Appendix A

$$\mathbf{M}_{uu} = 2m_{uu}R\int_0^L\int_0^{2\pi}\boldsymbol{\varphi}\boldsymbol{\varphi}^T dxd\theta \tag{A1}$$

$$\mathbf{M}_{uw} = m_{uw}R\int_0^L\int_0^{2\pi}\boldsymbol{\varphi}\frac{\partial\boldsymbol{\varpi}}{\partial\theta}^T dxd\theta \tag{A2}$$

$$\mathbf{M}_{ux} = m_{ux}R\int_0^L\int_0^{2\pi}\boldsymbol{\varphi}\boldsymbol{\vartheta}^T dxd\theta \tag{A3}$$

$$\mathbf{M}_{vv} = 2m_{vv}R\int_0^L\int_0^{2\pi}\boldsymbol{\psi}\boldsymbol{\psi}^T dxd\theta \tag{A4}$$

$$\mathbf{M}_{vw} = m_{vw}R\int_0^L\int_0^{2\pi}\boldsymbol{\psi}\frac{\partial\boldsymbol{\varpi}}{\partial\theta}^T dxd\theta \tag{A5}$$

$$\mathbf{M}_{v\theta} = m_{v\theta}R\int_0^L\int_0^{2\pi}\boldsymbol{\psi}\boldsymbol{\xi}^T dxd\theta \tag{A6}$$

$$\begin{aligned}\mathbf{M}_{ww} &= 2m_{ww1}R\int_0^L\int_0^{2\pi}\boldsymbol{\varpi}\boldsymbol{\varpi}^T dxd\theta\\ &+2m_{ww2}R\int_0^L\int_0^{2\pi}\frac{\partial\boldsymbol{\varpi}}{\partial x}\frac{\partial\boldsymbol{\varpi}}{\partial x}^T dxd\theta\\ &+2m_{ww3}R\int_0^L\int_0^{2\pi}\frac{\partial\boldsymbol{\varpi}}{\partial\theta}\frac{\partial\boldsymbol{\varpi}}{\partial\theta}^T dxd\theta\end{aligned} \tag{A7}$$

$$\mathbf{M}_{wx} = m_{wx}R\int_0^L\int_0^{2\pi}\frac{\partial\boldsymbol{\varpi}}{\partial x}\boldsymbol{\vartheta}^T dxd\theta \tag{A8}$$

$$\mathbf{M}_{w\theta} = m_{w\theta}R\int_0^L\int_0^{2\pi}\frac{\partial\boldsymbol{\varpi}}{\partial\theta}\boldsymbol{\xi}^T dxd\theta \tag{A9}$$

$$\mathbf{M}_{xx} = 2m_{xx}R\int_0^L\int_0^{2\pi}\boldsymbol{\vartheta}\boldsymbol{\vartheta}^T dxd\theta \tag{A10}$$

$$\mathbf{M}_{\theta\theta} = 2m_{\theta\theta}R\int_0^L\int_0^{2\pi}\boldsymbol{\xi}\boldsymbol{\xi}^T dxd\theta \tag{A11}$$

$$\begin{aligned}\mathbf{K}_{uu} &= A_{11}R\int_0^L\int_0^{2\pi}\frac{\partial\boldsymbol{\varphi}}{\partial x}\frac{\partial\boldsymbol{\varphi}}{\partial x}^T dxd\theta\\ &+\frac{A_{66}}{R}\int_0^L\int_0^{2\pi}\frac{\partial\boldsymbol{\varphi}}{\partial\theta}\frac{\partial\boldsymbol{\varphi}}{\partial\theta}^T dxd\theta\end{aligned} \tag{A12}$$

$$\begin{aligned}\mathbf{K}_{uv} &= A_{12}R\int_0^L\int_0^{2\pi}\frac{\partial\boldsymbol{\varphi}}{\partial x}\frac{\partial\boldsymbol{\psi}}{\partial\theta}^T dxd\theta\\ &+A_{66}\int_0^L\int_0^{2\pi}\frac{\partial\boldsymbol{\varphi}}{\partial\theta}\frac{\partial\boldsymbol{\psi}}{\partial x}^T dxd\theta\end{aligned} \tag{A13}$$

$$\begin{aligned}\mathbf{K}_{uw} &= A_{12}R\int_0^L\int_0^{2\pi}\frac{\partial\boldsymbol{\varphi}}{\partial x}\boldsymbol{\varpi}^T dxd\theta\\ &-c_1E_{11}R\int_0^L\int_0^{2\pi}\frac{\partial\boldsymbol{\varphi}}{\partial x}\frac{\partial^2\boldsymbol{\varpi}}{\partial x^2}^T dxd\theta\\ &-\frac{c_1E_{12}}{R}\int_0^L\int_0^{2\pi}\frac{\partial\boldsymbol{\varphi}}{\partial x}\frac{\partial^2\boldsymbol{\varpi}}{\partial\theta^2}^T dxd\theta\\ &-\frac{2c_1E_{66}}{R}\int_0^L\int_0^{2\pi}\frac{\partial\boldsymbol{\varphi}}{\partial\theta}\frac{\partial^2\boldsymbol{\varpi}}{\partial x\partial\theta}^T dxd\theta\end{aligned} \tag{A14}$$

$$\begin{aligned}\mathbf{K}_{ux} &= (B_{11}-c_1E_{11})R\int_0^L\int_0^{2\pi}\frac{\partial\boldsymbol{\varphi}}{\partial x}\frac{\partial\boldsymbol{\vartheta}}{\partial x}^T dxd\theta\\ &+(\frac{B_{66}}{R}-\frac{c_1E_{66}}{R})\int_0^L\int_0^{2\pi}\frac{\partial\boldsymbol{\varphi}}{\partial\theta}\frac{\partial\boldsymbol{\vartheta}}{\partial\theta}^T dxd\theta\end{aligned} \tag{A15}$$

$$\begin{aligned}\mathbf{K}_{u\theta} &= (B_{12}-c_1E_{12})R\int_0^L\int_0^{2\pi}\frac{\partial\boldsymbol{\varphi}}{\partial x}\frac{\partial\boldsymbol{\xi}}{\partial\theta}^T dxd\theta\\ &+(B_{66}-c_1E_{66})R\int_0^L\int_0^{2\pi}\frac{\partial\boldsymbol{\varphi}}{\partial\theta}\frac{\partial\boldsymbol{\xi}}{\partial x}^T dxd\theta\end{aligned} \tag{A16}$$

$$\begin{aligned}\mathbf{K}_{vv} &= A_{66}R\int_0^L\int_0^{2\pi}\frac{\partial\boldsymbol{\psi}}{\partial x}\frac{\partial\boldsymbol{\psi}}{\partial x}^T dxd\theta\\ &+\frac{A_{22}}{R}\int_0^L\int_0^{2\pi}\frac{\partial\boldsymbol{\psi}}{\partial y}\frac{\partial\boldsymbol{\psi}}{\partial y}^T dxd\theta\end{aligned} \tag{A17}$$

$$\begin{aligned}\mathbf{K}_{vw} &= \frac{A_{22}}{R}\int_0^L\int_0^{2\pi}\frac{\partial\boldsymbol{\psi}}{\partial\theta}\boldsymbol{\varpi}^T dxd\theta\\ &-\frac{c_1E_{22}}{R^2}\int_0^L\int_0^{2\pi}\frac{\partial\boldsymbol{\psi}}{\partial\theta}\frac{\partial^2\boldsymbol{\varpi}}{\partial\theta^2}^T dxd\theta\\ &-c_1E_{12}\int_0^L\int_0^{2\pi}\frac{\partial\boldsymbol{\psi}}{\partial\theta}\frac{\partial^2\boldsymbol{\varpi}}{\partial x^2}^T dxd\theta\\ &-2c_1E_{66}\int_0^L\int_0^{2\pi}\frac{\partial\boldsymbol{\psi}}{\partial x}\frac{\partial^2\boldsymbol{\varpi}}{\partial x\partial\theta}^T dxd\theta\end{aligned} \tag{A18}$$

$$\begin{aligned}\mathbf{K}_{vx} &= (B_{66}-c_1E_{66})\int_0^L\int_0^{2\pi}\frac{\partial\boldsymbol{\psi}}{\partial x}\frac{\partial\boldsymbol{\vartheta}}{\partial\theta}^T dxd\theta\\ &+(B_{12}-c_1E_{12})\int_0^L\int_0^{2\pi}\frac{\partial\boldsymbol{\psi}}{\partial\theta}\frac{\partial\boldsymbol{\vartheta}}{\partial x}^T dxd\theta\end{aligned} \tag{A19}$$

$$\begin{aligned}\mathbf{K}_{v\theta} &= \left(\frac{B_{22}}{R}-\frac{c_1E_{22}}{R}\right)\int_0^L\int_0^{2\pi}\frac{\partial\boldsymbol{\psi}}{\partial\theta}\frac{\partial\boldsymbol{\xi}}{\partial\theta}^T dxd\theta\\ &+(B_{66}-c_1E_{66})R\int_0^L\int_0^{2\pi}\frac{\partial\boldsymbol{\psi}}{\partial x}\frac{\partial\boldsymbol{\xi}}{\partial x}^T dxd\theta\end{aligned} \tag{A20}$$

$$
\begin{aligned}
&\mathbf{K}_{ww}\\
&=(c_2^2F_{55}+A_{55}-2c_2D_{55})R\int_0^L\int_0^{2\pi}\frac{\partial\boldsymbol{\varpi}}{\partial x}\frac{\partial\boldsymbol{\varpi}}{\partial x}^T\,dxd\theta\\
&+\frac{c_2^2F_{44}+A_{44}-2c_2D_{44}}{R}\int_0^L\int_0^{2\pi}\frac{\partial\boldsymbol{\varpi}}{\partial\theta}\frac{\partial\boldsymbol{\varpi}}{\partial\theta}^T\,dxd\theta\\
&+\frac{4c_1^2H_{66}}{R}\int_0^L\int_0^{2\pi}\frac{\partial^2\boldsymbol{\varpi}}{\partial x\partial\theta}\frac{\partial^2\boldsymbol{\varpi}}{\partial x\partial\theta}^T\,dxd\theta\\
&+\frac{c_1^2H_{22}}{R^3}\int_0^L\int_0^{2\pi}\frac{\partial^2\boldsymbol{\varpi}}{\partial\theta^2}\frac{\partial^2\boldsymbol{\varpi}}{\partial\theta^2}^T\,dxd\theta\\
&+\frac{A_{22}}{R}\int_0^L\int_0^{2\pi}\boldsymbol{\varpi}\boldsymbol{\varpi}^{\boldsymbol{T}}dxd\theta\\
&+c_1^2H_{11}R\int_0^L\int_0^{2\pi}\frac{\partial^2\boldsymbol{\varpi}}{\partial x^2}\frac{\partial^2\boldsymbol{\varpi}}{\partial x^2}^T\,dxd\theta\\
&+\frac{c_1^2H_{12}}{R}\int_0^L\int_0^{2\pi}(\frac{\partial^2\boldsymbol{\varpi}}{\partial x^2}\frac{\partial^2\boldsymbol{\varpi}}{\partial\theta^2}^T+\frac{\partial^2\boldsymbol{\varpi}}{\partial\theta^2}\frac{\partial^2\boldsymbol{\varpi}}{\partial x^2}^T)dxd\theta\\
&-c_1E_{12}\int_0^L\int_0^{2\pi}(\frac{\partial^2\boldsymbol{\varpi}}{\partial x^2}\boldsymbol{\varpi}^{\boldsymbol{T}}+\boldsymbol{\varpi}\frac{\partial^2\boldsymbol{\varpi}}{\partial x^2}^T)dxd\theta\\
&-\frac{c_1^2E_{22}}{R^2}\int_0^L\int_0^{2\pi}(\frac{\partial^2\boldsymbol{\varpi}}{\partial\theta^2}\boldsymbol{\varpi}^{\boldsymbol{T}}+\boldsymbol{\varpi}\frac{\partial^2\boldsymbol{\varpi}}{\partial\theta^2}^T)dxd\theta
\end{aligned}
\tag{A21}
$$

$$
\begin{aligned}
&\mathbf{K}_{wx}\\
&=c_1(c_1H_{66}-F_{11})R\int_0^L\int_0^{2\pi}\frac{\partial^2\boldsymbol{\varpi}}{\partial x^2}\frac{\partial\boldsymbol{\vartheta}}{\partial x}^T\,dxd\theta\\
&+(c_2^2F_{55}-2c_2D_{55}+A_{55})\int_0^L\int_0^{2\pi}\frac{\partial\boldsymbol{\varpi}}{\partial x}\boldsymbol{\vartheta}^T dxd\theta\\
&+\frac{2c_1(c_1H_{66}-F_{66})}{R}\int_0^L\int_0^{2\pi}\frac{\partial^2\boldsymbol{\varpi}}{\partial x\partial\theta}\frac{\partial\boldsymbol{\vartheta}}{\partial\theta}^T\,dxd\theta\\
&+\frac{c_1(c_1H_{12}-F_{66})}{R}\int_0^L\int_0^{2\pi}\frac{\partial^2\boldsymbol{\varpi}}{\partial\theta^2}\frac{\partial\boldsymbol{\vartheta}}{\partial x}^T\,dxd\theta\\
&+(B_{12}-c_1E_{12})\int_0^L\int_0^{2\pi}\boldsymbol{\varpi}\frac{\partial\boldsymbol{\vartheta}}{\partial x}^T\,dxd\theta
\end{aligned}
\tag{A22}
$$

$$
\begin{aligned}
&\mathbf{K}_{w\theta}\\
&=c_1(c_1H_{12}-F_{12})\int_0^L\int_0^{2\pi}\frac{\partial^2\boldsymbol{\varpi}}{\partial x^2}\frac{\partial\boldsymbol{\xi}}{\partial\theta}^T\,dxd\theta\\
&+(c_2^2F_{44}-2c_2D_{44}+A_{44})\int_0^L\int_0^{2\pi}\frac{\partial\boldsymbol{\varpi}}{\partial x}\boldsymbol{\xi}^T dxd\theta\\
&+2c_1(c_1H_{66}-F_{66})\int_0^L\int_0^{2\pi}\frac{\partial^2\boldsymbol{\varpi}}{\partial x\partial\theta}\frac{\partial\boldsymbol{\xi}}{\partial x}^T\,dxd\theta\\
&+\frac{c_1(c_1H_{12}-F_{22})}{R^2}\int_0^L\int_0^{2\pi}\frac{\partial^2\boldsymbol{\varpi}}{\partial\theta^2}\frac{\partial\boldsymbol{\xi}}{\partial\theta}^T\,dxd\theta\\
&+\frac{(B_{12}-c_1E_{12})}{R}\int_0^L\int_0^{2\pi}\frac{\partial\boldsymbol{\varpi}}{\partial\theta}\boldsymbol{\xi}^{\boldsymbol{T}}dxd\theta
\end{aligned}
\tag{A23}
$$

$$
\begin{aligned}
&\mathbf{K}_{xx}\\
&=(c_1^2H_{11}-2c_1F_{11}+D_{11})R\int_0^L\int_0^{2\pi}\frac{\partial\boldsymbol{\vartheta}}{\partial x}\frac{\partial\boldsymbol{\vartheta}}{\partial x}^T\,dxd\theta\\
&+\frac{c_2^2H_{66}-2c_2F_{66}+D_{66}}{R}\int_0^L\int_0^{2\pi}\frac{\partial\boldsymbol{\vartheta}}{\partial\theta}\frac{\partial\boldsymbol{\vartheta}}{\partial\theta}^T\,dxd\theta\\
&+(c_2^2F_{55}-2c_2D_{55}+A_{55})R\int_0^L\int_0^{2\pi}\boldsymbol{\vartheta}\boldsymbol{\vartheta}^{\boldsymbol{T}}dxd\theta
\end{aligned}
\tag{A24}
$$

$$
\begin{aligned}
&\mathbf{K}_{xx}\\
&=(c_1^2H_{11}-2c_1F_{11}+D_{11})R\int_0^L\int_0^{2\pi}\frac{\partial\boldsymbol{\vartheta}}{\partial x}\frac{\partial\boldsymbol{\vartheta}}{\partial x}^T\,dxd\theta\\
&+\frac{c_2^2H_{66}-2c_2F_{66}+D_{66}}{R}\int_0^L\int_0^{2\pi}\frac{\partial\boldsymbol{\vartheta}}{\partial\theta}\frac{\partial\boldsymbol{\vartheta}}{\partial\theta}^T\,dxd\theta\\
&+(c_2^2F_{55}-2c_2D_{55}+A_{55})R\int_0^L\int_0^{2\pi}\boldsymbol{\vartheta}\boldsymbol{\vartheta}^{\boldsymbol{T}}dxd\theta
\end{aligned}
\tag{A25}
$$

$$
\begin{aligned}
&\mathbf{K}_{\theta\theta}\\
&=(c_1^2H_{66}-2c_1F_{66}+D_{66})R\int_0^L\int_0^{2\pi}\frac{\partial\boldsymbol{\xi}}{\partial x}\frac{\partial\boldsymbol{\xi}}{\partial x}^T\,dxd\theta\\
&+\frac{c_1^2H_{22}-2c_1F_{22}+D_{22}}{R}\int_0^L\int_0^{2\pi}\frac{\partial\boldsymbol{\xi}}{\partial\theta}\frac{\partial\boldsymbol{\xi}}{\partial\theta}^T\,dxd\theta\\
&+(c_2^2F_{44}-2c_2D_{44}+A_{44})R\int_0^L\int_0^{2\pi}\boldsymbol{\xi}\boldsymbol{\xi}^{\boldsymbol{T}}dxd\theta
\end{aligned}
\tag{A26}
$$

$$
\begin{aligned}
&\mathbf{K}_{\theta\theta}\\
&=(c_1^2H_{66}-2c_1F_{66}+D_{66})R\int_0^L\int_0^{2\pi}\frac{\partial\boldsymbol{\xi}}{\partial x}\frac{\partial\boldsymbol{\xi}}{\partial x}^T\,dxd\theta\\
&+\frac{c_1^2H_{22}-2c_1F_{22}+D_{22}}{R}\int_0^L\int_0^{2\pi}\frac{\partial\boldsymbol{\xi}}{\partial\theta}\frac{\partial\boldsymbol{\xi}}{\partial\theta}^T\,dxd\theta\\
&+(c_2^2F_{44}-2c_2D_{44}+A_{44})R\int_0^L\int_0^{2\pi}\boldsymbol{\xi}\boldsymbol{\xi}^{\boldsymbol{T}}dxd\theta
\end{aligned}
\tag{A27}
$$

Appendix B

$$m_{uu} = \frac{1}{2}h(V^*\rho^{CNT} - V^*\rho^m + \rho^m) \tag{B1}$$

$$m_{ux} = 0, \quad m_{uv} = 0 \tag{B2}$$

$$m_{vv} = \frac{1}{2}h(\rho^m + V^*\rho^{CNT} - V^*\rho^m) + \frac{1}{48}\frac{h^3}{R^2}(2\rho^m - 3V^*\rho^m + 3V^*\rho^{CNT}) \tag{B3}$$

$$m_{vv} = \frac{1}{240}\frac{c_1 h^5}{R^2}(5V^*\rho^m - 5V^*\rho^{CNT} - 3\rho^m) \tag{B4}$$

$$m_{v\theta} = \frac{1}{240}\frac{c_1 h^5}{R^2}(5V^*\rho^m - 5V^*\rho^{CNT} - 3\rho^m) + 24\frac{h^3}{R}(2\rho^m + 3V^*\rho^{CNT} - 3V^*\rho^m) \tag{B5}$$

$$m_{ww1} = \frac{1}{2}h(V^*\rho^{CNT} - V^*\rho^m + \rho^m) \tag{B6}$$

$$m_{ww2} \approx 0, \quad m_{ww3} \approx 0 \tag{B7}$$

$$m_{xx} = \frac{1}{24}h^3\rho^m - \frac{1}{80}c_1 h^5\rho^m + \frac{1}{16}h^3V^*\rho^{CNT} - \frac{1}{16}h^3V^*\rho^m + \frac{1}{48}c_1 h^5V^*\rho^m - \frac{1}{48}c_1 h^5V^*\rho^{CNT} \tag{B8}$$

$$m_{\theta\theta} = \frac{1}{24}h^3\rho^m - \frac{1}{80}c_1 h^5\rho^m + \frac{1}{16}h^3V^*\rho^{CNT} - \frac{1}{16}h^3V^*\rho^m + \frac{1}{48}c_1 h^5V^*\rho^m - \frac{1}{48}c_1 h^5V^*\rho^{CNT} \tag{B9}$$